



Cite this: *Environ. Sci.: Atmos.*, 2023, **3**, 1174

## Different chlorine and hydroxyl radical environments impact *m*-xylene oxidation products†

Nirvan Bhattacharyya, Mrinali Modi, Leif G. Jahn and Lea Hildebrandt Ruiz \*

Airborne emissions of aromatic hydrocarbons including benzene, ethylbenzene, toluene, and xylenes are associated with anthropogenic activities (e.g. transportation) and form secondary organic aerosol (SOA) when oxidized. While hydroxyl radicals (OH) dominate oxidation, chlorine radicals (Cl) react with alkyl substituted aromatics more rapidly and favor a different oxidative pathway. High concentrations of reactive chlorine species have been observed in continental and coastal regions, where mixed Cl/OH chemistry is expected to influence regional SOA formation and composition. This study uses environmental chamber experiments to assess SOA formation and composition from the oxidation of *m*-xylene in mixed Cl/OH oxidation environments. Experiments were conducted with hydrogen peroxide ( $H_2O_2$ ), chlorine ( $Cl_2$ ), and nitryl chloride ( $ClNO_2$ ) radical precursors under high and low  $NO_x$  conditions. Data was collected with an Aerosol Chemical Speciation Monitor (ACSM), Scanning Electrical Mobility System (SEMS) and time of flight chemical ionization mass spectrometer with filter desorption (FIGAERO-CIMS) utilizing  $H_3O^+$  and  $I^-$  reagent ions. Different oxidative pathways in  $H_2O_2$  and  $Cl_2$  experiments resulted in bicyclic peroxide and methylbenzoquinone species, respectively. When  $Cl_2$  was the sole radical precursor, SOA was more highly oxidized and less fragmented.  $ClNO_2$  experiments formed substantial amounts of bicyclic peroxide and minimal methylbenzoquinone in the gas phase and less oxidized SOA with a lower fraction of organochlorides. These differences are related to secondary OH formation and slower  $ClNO_2$  photolysis driving lower Cl radical concentrations. This study provides evidence that gas and particle-phase products vary depending on the oxidative environment and underlines the importance of studying novel oxidants and oxidative pathways.

Received 17th February 2023  
Accepted 27th May 2023

DOI: 10.1039/d3ea00024a  
[rsc.li/esatmospheres](http://rsc.li/esatmospheres)

### Environmental significance

Aromatic hydrocarbon oxidation forms atmospheric aerosols which impact health and climate. Previous environmental chamber studies focus on OH radical oxidation, but Cl radicals react faster with alkyl substituted aromatics along an alternate reaction pathway. Experiments with  $H_2O_2$ ,  $Cl_2$ , and  $ClNO_2$  examine gas phase chemistry, particle formation, and product composition from oxidation of *m*-xylene. We demonstrate OH and Cl oxidation results in different products. More highly oxidized organic aerosol is formed in experiments when only  $Cl_2$  is a radical precursor. Using  $ClNO_2$  as a radical precursor results in different chemistry and product distributions than  $Cl_2 + NO_x$ , indicating  $ClNO_2$ -laden air reacts differently than  $Cl_2$  emissions in high  $NO_x$  environments. Exploration of radical precursors is required to constrain Cl oxidation impacts.

## 1 Introduction

Aromatic hydrocarbons are a substantial fraction of volatile organic compound (VOC) emissions globally and regionally.<sup>1-3</sup> In urban environments, small aromatics including benzene, toluene, ethylbenzene, and xylenes (BTEX) often dominate observed VOCs, and their main source is thought to be transportation.<sup>4,5</sup>

Atmospheric oxidation of these species leads to substantial formation of ozone, oxidized volatile organic compounds (OVOCs),<sup>6,7</sup> and secondary organic aerosol (SOA).<sup>8-10</sup> SOA impacts climate forcing<sup>11</sup> and human health,<sup>12</sup> and a complete understanding of formation mechanisms is necessary to evaluate policy options to reduce SOA. Environmental chamber experiments on hydroxyl radical (OH) oxidation of BTEX compounds show SOA yields ranging from 5–40% dependent on seed aerosol,  $NO_x$  concentration, and relative humidity (RH).<sup>10,13-15</sup> Estimated SOA production from these aromatics ranges from 2–12 Tg annually.<sup>9</sup>

While hydroxyl radicals (OH) are the most abundant radical in the atmosphere and are thought to dominate aromatic

McKetta Department of Chemical Engineering, The University of Texas at Austin, Austin, TX 78712, USA. E-mail: [lhr@che.utexas.edu](mailto:lhr@che.utexas.edu)

† Electronic supplementary information (ESI) available. See DOI: <https://doi.org/10.1039/d3ea00024a>

hydrocarbon oxidation,<sup>10,16</sup> chlorine radicals (Cl) may also have a substantial impact due to their more rapid reaction rate with substituted aromatic hydrocarbons.<sup>17</sup> However, atmospheric Cl radical concentrations have been historically underestimated and consequently understudied.<sup>18</sup> Rapid oxidation by Cl may enhance SOA formation due to rapid formation of semivolatile organic compounds (SVOCs).<sup>10,19</sup> In addition, while OH radicals add to the aromatic ring in over 90% of initial oxidations,<sup>7,20</sup> Cl radicals perform hydrogen abstraction from alkyl substituents on the aromatic ring.<sup>17,21</sup> Previous work on toluene + Cl oxidation has illustrated differences in gas phase products compared to OH radical oxidation including formation of aldehyde, peroxy acid, and quinone species.<sup>22</sup> Particles were more highly oxidized from Cl-initiated chemistry than from OH-initiated reactions, and chlorinated species were observed.<sup>22,23</sup>

Prior work on chlorine oxidation typically utilized molecular chlorine ( $\text{Cl}_2$ ) as the chlorine radical precursor.<sup>22–27</sup> While  $\text{Cl}_2$  has been observed far inland of marine and coastal sources including in urban environments,<sup>28,29</sup> nitryl chloride ( $\text{ClNO}_2$ ) is often more abundant than  $\text{Cl}_2$  in these environments, particularly in early morning air masses.<sup>30</sup> Near oil and gas production well sites,  $\text{Cl}_2$  concentrations were observed to be higher than  $\text{ClNO}_2$ .<sup>31</sup> Atmospheric sources of  $\text{Cl}_2$  are largely associated with industrial emissions and biocides, though some heterogenous reactions on chloride aerosols have been shown to produce  $\text{Cl}_2$ .<sup>32,33</sup>  $\text{ClNO}_2$  is primarily produced from heterogeneous reaction of dinitrogen pentoxide ( $\text{N}_2\text{O}_5$ ) with particulate or aqueous chloride from sources including sea salt aerosol, biomass burning aerosol, saline snowpack, playa dusts, and aerosol in polluted megacities.<sup>34–37</sup> Beyond being an atmospherically relevant Cl source,  $\text{ClNO}_2$  photolysis generates  $\text{NO}_2$ , which photolyses to NO. Under these high  $\text{NO}_x$  conditions, Cl radical oxidation leads to formation of secondary OH radicals as NO reacts with  $\text{HO}_2$ .<sup>38</sup> Secondary hydroxyl radical production under high  $\text{NO}_x$  conditions has been shown to obscure the impact of Cl radicals from traditional VOC decay techniques for assessing Cl radical concentrations.<sup>39</sup> Furthermore, the presence of  $\text{NO}_x$  suppresses SOA formation from aromatics due to a shift in peroxy radical fate and subsequent fragmentation.<sup>10,14,40</sup> Nitryl chloride generates a complex mixture of radicals and oxidants with substantial impacts on gas phase chemistry, SOA formation, and SOA composition.

Here, we evaluate the impacts of different oxidative environments on the formation of gas and particle phase products from the oxidation of *m*-xylene in an environmental chamber. We utilize chlorine gas, nitryl chloride, and hydrogen peroxide as radical precursors under high and low  $\text{NO}_x$  conditions, generating environments in which only OH, only Cl or a mixture of both radicals are initiating oxidation of hydrocarbons. These different oxidative environments have substantial impacts on gas and particle phase products and composition. We observe and discuss the formation of several gas phase products, and evaluate chemically-specified particle composition using a thermal desorption technique. We also assess SOA mass yield and bulk composition.

## 2 Methods

### 2.1 Chamber photo-oxidation experiments

Oxidation experiments were conducted in a 10 m<sup>3</sup> Teflon environmental chamber at 298 K at 30% relative humidity (RH) using UV black lights with a peak emission at 354 nm to generate radicals. Clean dry air was supplied to the chamber using a clean-air generator (model 727R, AADCO). The chamber was flushed overnight with humidified clean air to reach the target 30% RH. Dried ammonium sulfate seed particles were generated from 0.05 M aqueous ammonium sulfate injected with an aerosol generation system (AGS 2002, Brechtel). Chlorine gas (100.3 ppm in N<sub>2</sub>, Airgas) was directly injected into the chamber. Multipoint calibrations of the I<sup>–</sup> CIMS for  $\text{Cl}_2$  were performed based on repeated injections into the chamber. Nitryl chloride was generated reactively by passing  $\text{Cl}_2$  (100.3 ppm in N<sub>2</sub>) at a low flow rate (0.25 L min<sup>–1</sup>) over a solution of sodium nitrite as previously described.<sup>41</sup> Based on data from the iodide mode chemical ionization mass spectrometer (I<sup>–</sup> CIMS), >99% of  $\text{Cl}_2$  is consumed at this flow rate (<1% of initial  $\text{Cl}_2$  signal remains) and for calibration purposes, it is assumed that 100% of  $\text{Cl}_2$  injected is converted to  $\text{ClNO}_2$  during  $\text{ClNO}_2$  injection to the chamber. Formation of the common  $\text{NO}_2$  byproduct during  $\text{ClNO}_2$  synthesis is not observed in this study. Multipoint I<sup>–</sup> CIMS calibration for  $\text{ClNO}_2$  was performed based on repeated injection into the chamber based on this 100% conversion. Hydrogen peroxide was injected as an OH radical

Table 1 List of experimental conditions, SOA formation, and selected organic yields

#	Radical precursors	[VOC] <sub>0</sub> (μg m <sup>–3</sup> )	[Cl <sub>2</sub> ] <sub>0</sub> (ppb)	[ClNO <sub>2</sub> ] <sub>0</sub> (ppb)	[H <sub>2</sub> O <sub>2</sub> ] <sub>0</sub> (ppm)	[NO <sub>x</sub> ] <sub>0</sub> (ppb)	Max SOA <sup>a</sup> (μg m <sup>–3</sup> )	Yield <sup>b</sup> (%)
1	ClNO <sub>2</sub>	340	<0.1	50	<0.1	<2	— <sup>c</sup>	—
2	ClNO <sub>2</sub>	340	<0.1	50	<0.1	<2	12.7	4.8
3	Cl <sub>2</sub> + NO <sub>x</sub>	340	25	<0.1	<0.1	20	12.0	—
4	Cl <sub>2</sub>	340	25	<0.1	<0.1	<2	24.3	8.8
5	Cl <sub>2</sub>	340	25	<0.1	<0.1	<2	— <sup>c</sup>	—
6	H <sub>2</sub> O <sub>2</sub> + NO <sub>x</sub>	340	<0.1	<0.1	1	20	10.1	4.4
7	H <sub>2</sub> O <sub>2</sub>	340	<0.1	<0.1	1	<2	11.2	—
8	Cl <sub>2</sub> + ClNO <sub>2</sub>	340	10	30	<0.1	<2	11.3	—
9	Cl <sub>2</sub> + H <sub>2</sub> O <sub>2</sub>	340	10	<0.1	1	<2	— <sup>c</sup>	—
10	Cl <sub>2</sub> + ClNO <sub>2</sub> + H <sub>2</sub> O <sub>2</sub>	340	5	15	1	<2	10.1	—

<sup>a</sup> Peak SOA is calculated based on wall loss corrected ACSM organic loading following the UV illumination period. <sup>b</sup> Yield (organic aerosol mass yield) is calculated for experiments where H<sub>3</sub>O<sup>+</sup> CIMS data are available to measure xylene consumption. <sup>c</sup> Aerosol data unavailable for this experiment.



precursor by bubbling clean dry air at  $2 \text{ L min}^{-1}$  through a 30% hydrogen peroxide solution (Sigma Aldrich) for 1 hour. Hydrogen peroxide concentration was estimated at 1 ppm based on interference in the 254 nm photometric ozone monitor and the relative ratios of the absorption cross sections of ozone and hydrogen peroxide at 254 nm.  $\text{I}^-$  CIMS measurements of hydrogen peroxide injection indicated that injections were repeatable, and response was linear with respect to injection volume. *m*-Xylene (>99% purity, Sigma Aldrich) was injected into a glass gas sampling tube which was flushed into the chamber with heated clean air at  $2 \text{ L min}^{-1}$  for 30 minutes. Complete vaporization and injection of *m*-xylene into the chamber is assumed in calculating initial concentrations. Nitric acid (NO) (50.3 ppm in  $\text{N}_2$ , Airgas) was directly injected into the chamber for high  $\text{NO}_x$  experiments. Initial VOC and oxidant precursor concentrations are listed in Table 1.

An example experimental time series is shown in Fig. 1. Following injection, VOCs, oxidant precursors, and seeds were allowed to mix and then UV lights were turned on (time = 0 in Fig. 1) to initiate photo-oxidation.  $\text{Cl}_2$  (or other radical precursors) are photolyzed to form radicals which oxidize *m*-xylene to form oxidation products including SOA and O VOCs. Photo-oxidation continued for 1 to 2 hours until organic aerosol concentrations stabilized. Organic aerosol concentrations stabilized earlier for  $\text{Cl}_2$  experiments due to its rapid photolysis rate compared to  $\text{ClNO}_2$  and  $\text{H}_2\text{O}_2$ . *m*-Xylene was typically not completely consumed. "Blank" experiments were conducted the day before and after photo-oxidation experiments where only oxidant precursors and ammonium sulfate seed were present. Minimal SOA formation ( $<1 \mu\text{g m}^{-3}$ ) was observed in "blank" experiments.

## 2.2 Instrumentation

NO and total  $\text{NO}_x$  concentrations were monitored with a chemiluminescent monitor (200E, Teledyne); limit of detection (LOD)

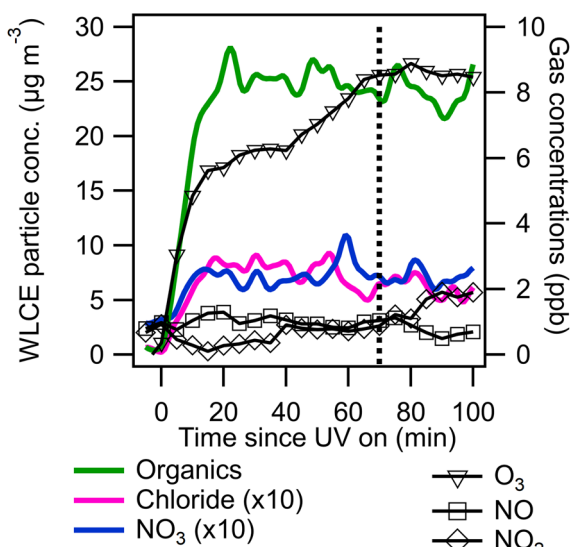


Fig. 1 Experiment 4 ( $\text{Cl}_2$ ) wall loss and collection efficiency corrected (WLCE) ACSM data (left axis) and trace gas monitor data (right axis). Chloride and nitrate traces are multiplied by 10 for legibility. Vertical dashed line indicates end of UV light on period.

0.4 ppb and  $\pm 0.2$  ppb accuracy.  $\text{NO}_2$  concentrations were measured directly using a monitor from Environnement (Model AS32M) using a cavity attenuated phase shift (CAPS) method; LOD 0.1 ppb and  $\pm 0.05$  ppb accuracy. Ozone concentrations were monitored with a photometric ozone analyzer (400E, Teledyne); LOD 0.6 ppb and  $\pm 0.3$  ppb accuracy. Particle size distributions in the 10–1000 nm size range were measured using a scanning electrical mobility system (SEMS, Brechtel model 2002). Bulk particle phase composition was assessed using an aerosol chemical speciation monitor (ACSM, Aerodyne),<sup>42</sup> calibrated with 300 nm size-selected ammonium nitrate and ammonium sulfate particles. Particle phase concentrations from the ACSM were corrected for chamber wall losses and instrument collection efficiency by taking the ratio of organic to sulfate signal and multiplying by the initial ammonium sulfate seed concentration measured by the SEMS data as previously described.<sup>15</sup> Wall loss and collection efficiency corrected (WLCE) ACSM data were used to calculate SOA yield for experiments 2, 4, and 6 where *m*-xylene consumption was measured by switching the CIMS reagent ion to the positive hydronium ion ( $\text{H}_3\text{O}^+$  CIMS). A single CIMS system was utilized in this study and was switched between negative ( $\text{I}^-$ ) and positive ( $\text{H}_3\text{O}^+$ ) modes for some experiments. SOA yield was calculated as the change in wall loss corrected ACSM organic mass from before and after the UV photo-oxidation period divided by the mass of *m*-xylene consumed.

Gas and particle phase composition was assessed using a Filter Inlet for Gases and Aerosols coupled to an iodide mode chemical ionization mass spectrometer (FIGAERO-CIMS, Aerodyne). Iodide mode FIGAERO-CIMS has been described in detail elsewhere.<sup>43,44</sup> In this application, real time gas phase chemistry was observed using  $\text{I}^-$  CIMS including the decay of oxidant precursors and the formation of oxidized VOCs. In addition,  $\text{H}_3\text{O}^+$  CIMS was utilized to examine the decay of *m*-xylene during some oxidation experiments. Following UV photooxidation, lights were turned off and particles were collected on the FIGAERO-CIMS PTFE filter (1  $\mu\text{m}$  pore Zefon filters) at 3 SLPM for 45 minutes. Filters were desorbed using heated  $\text{N}_2$  (Airgas) which began at 25 °C and was heated to 300 °C over 30 minutes and held at 300 °C for 10 minutes. This particle desorption method allows for detailed speciation of a wide range of particle phase organic species.

For both gas and particle phase analysis of CIMS, high resolution peak fitting and identification was performed using the Tofware data analysis package. For  $\text{I}^-$  CIMS, all identified species are iodide adducts (elemental formula contains  $\text{I}^-$ ) and it is assumed that  $\text{I}^-$  is from ionization in the instrument and was not present on the analyte. Similarly,  $\text{H}^+$  or  $\text{H}_3\text{O}^+$  adducts are formed in positive mode CIMS. CIMS can only provide elemental compositions without information about molecular structure. When species are discussed, their likely structures are inferred based on expected reaction mechanisms and products.  $\text{I}^-$  CIMS calibration was performed as described above for radical precursor species ( $\text{H}_2\text{O}_2$ ,  $\text{Cl}_2$ , and  $\text{ClNO}_2$ ). Such calibrations were performed within 6 weeks of the experiment to which they were applied. All other species detected in the  $\text{I}^-$  CIMS are presented normalized to  $\text{I}^-$  reagent ion signal where analyte signal is divided at each time point by  $\text{I}^-$  signal and multiplied by 100 000. This normalization procedure adjusts for variability in reagent



ion concentration.  $\text{I}^-$  reagent ion signal varied by 10–30% during experiments, particularly during  $\text{Cl}_2$  experiments as  $\text{Cl}_2$  depletes  $\text{I}^-$  reagent ion.  $\text{I}^-$  CIMS sensitivity is also highly dependent on sample humidity.<sup>43</sup> To stabilize instrument response, reagent ion flow is humidified to above 70% RH by bubbling the reagent ion source  $\text{N}_2$  through purified water (MilliQ water purification system, ThermoScientific). Based on prior literature,<sup>43</sup>  $\text{I}^-$  CIMS limits of detection for compounds discussed here are in the 10 s of ppt or lower and accuracy is within  $\pm 10$  ppt.

Particle phase data from the FIGAERO is background subtracted and then integrated across the full thermal desorption period. In several cases, species are discussed and grouped based on their elemental composition. For example, organochlorine species with the composition  $\text{C}_{2-10}\text{H}_y\text{O}_z\text{Cl}_{1-3}\text{I}^-$  are discussed and consist of the total summed signal of all species which contain 2 to 10 carbon atoms, 1 or more hydrogen, 1 or more oxygen, and 1 to 3 chlorine atoms.

### 2.3 Chamber box modeling

A chamber box model utilizing the Carbon Bond Mechanism (version 6, revision 4) from the Comprehensive Air Quality Model with Extensions (CAMx)<sup>45</sup> with previously described modifications for chlorine radical chemistry<sup>46</sup> was used to model these experiments. Radical precursor, *m*-xylene,  $\text{NO}_x$ , temperature, and humidity concentrations were initialized in the model. UV light intensity in the model is based on previously measured blacklight spectra (P-200 spectroradiometer, Apogee Instruments). Chamber characterization experiments<sup>47</sup> provided measured  $\text{NO}_2$  photolysis rates, chamber leak rate ( $\text{Cl}_2$  utilized as a leak tracer), and wall effects. Modeling was used to capture  $\text{OH}$  and  $\text{Cl}$  radical concentrations. Fig. 2a–c shows measured and modeled consumption of radical precursors alongside modeled *m*-xylene consumption for low  $\text{NO}_x$   $\text{Cl}_2$ ,  $\text{ClNO}_2$ , and  $\text{H}_2\text{O}_2$  experiments. Model results indicate that  $\text{Cl}_2$  is rapidly consumed, while  $\text{ClNO}_2$  and  $\text{H}_2\text{O}_2$  have much slower modeled rates of consumption due to a lower photolysis rate under chamber lighting conditions. While chlorine consumption shows good model agreement, nitryl chloride consumption deviates slightly and hydrogen peroxide consumption deviates substantially from model predictions. This difference in modeled and measured radical precursor decay may be due to uncertainties associated with the measured UV spectrum. The absorption cross sections of  $\text{H}_2\text{O}_2$  and  $\text{ClNO}_2$  overlap only slightly with the measured emission spectrum of the UV lights and small errors in spectrum or absorption cross section measurements may substantially alter modeled photolysis rates. Absorption cross sections for radical precursors and the measured light spectrum used in the chamber model are shown in Fig. S1.†

## 3 Results and discussion

### 3.1 Radical precursor identity alters gas phase products and degree of oxidation

Chlorine and hydroxyl radicals utilize different primary oxidation pathways as illustrated in Schemes 1 (Cl) and 2 (OH). Three selected products illustrate these reaction pathway differences: 2-methyl-1,4-benzoquinone is formed primarily through

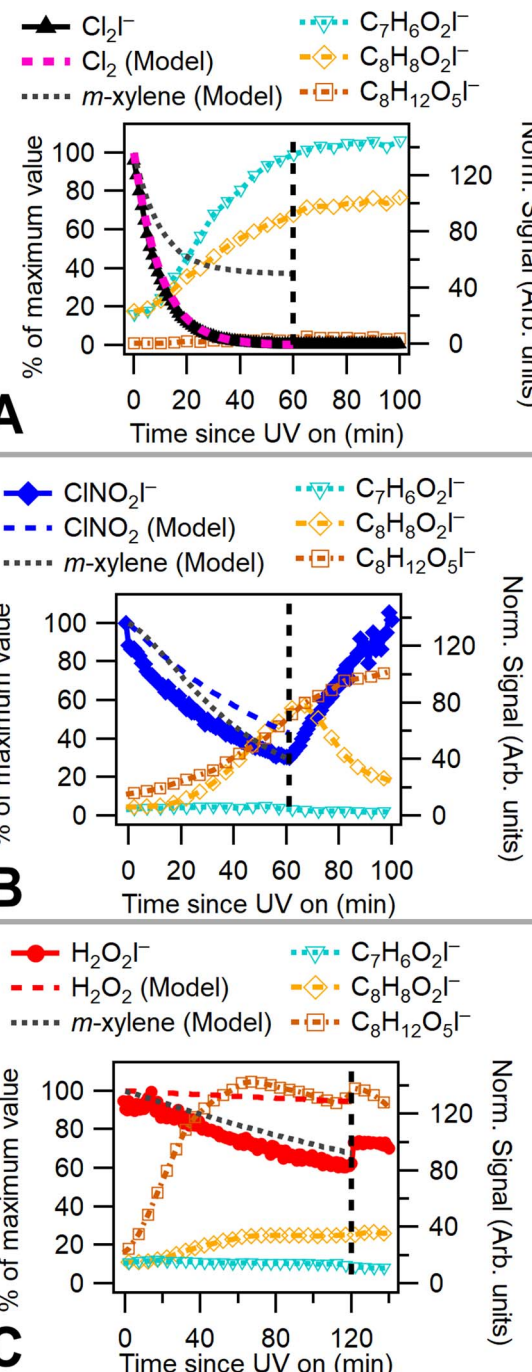
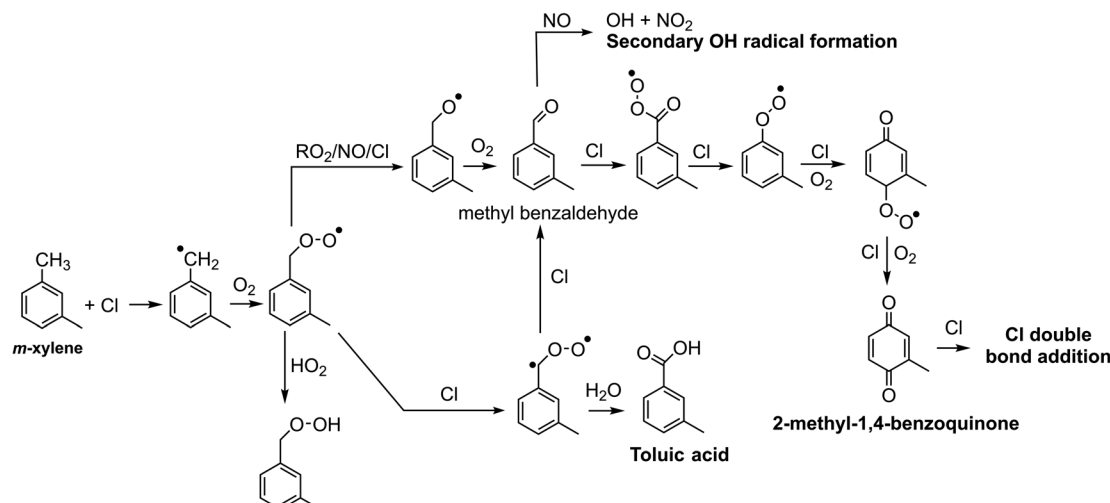


Fig. 2 (A)–(C) Normalized  $\text{I}^-$  CIMS data and chamber model results from (A) experiment 5 –  $\text{Cl}_2$  (B) experiment 1 –  $\text{ClNO}_2$  (C) experiment 7 –  $\text{H}_2\text{O}_2$ . Model and radical precursor time series are normalized to maximum value. Vertical dashes show UV lights were turned off.  $\text{C}_7\text{H}_6\text{O}_2\text{I}^-$  is consistent with 2-methyl-1,4-benzoquinone,  $\text{C}_8\text{H}_8\text{O}_2\text{I}^-$  with *m*-toluic acid, and  $\text{C}_8\text{H}_{12}\text{O}_5\text{I}^-$  with bicyclic peroxide.

hydrogen abstraction by the Cl radical, the bicyclic peroxide is formed from OH radical addition, and *m*-toluic acid can be formed by both radicals. Formation of these products is described briefly here.

Chlorine initiated oxidation of toluene forms 1,4-benzoquinone due to hydrogen abstraction of aldehydic hydrogen and



Scheme 1 Selected oxidation pathways for *m*-xylene + Cl.

additional Cl radical attack on peroxy radicals to form ClO.<sup>22,23,48</sup> Applying this reaction pathway to *m*-xylene predicts the analogous species, 2-methyl-1,4-benzoquinone ( $C_7H_6O_2$ ) measured here. Hydroxyl radicals can form quinone species through an OH ring addition pathway resulting in methyl phenol products, though this pathway is less common.<sup>49,50</sup>

The OH ring addition pathway generates a bicyclic radical species with a wide variety of fates, including epoxidation, fragmentation, and the bicyclic peroxide product ( $C_8H_{12}O_5$ )<sup>20,51</sup>

discussed here. Chlorine oxidation is not observed to cause ring addition and bicyclic radical species are not formed.<sup>17</sup>

Toluic acid is the result of hydrogen abstraction at the methyl group resulting in the carboxylic acid species. OH and Cl radicals form this product following attack on an aldehydic hydrogen. In addition, Cl oxidation generates toluic acid after forming a Criegee intermediate. Criegee intermediates form following the attack of chlorine on the peroxy radical<sup>52</sup> and have been previously discussed for toluene + Cl systems.<sup>53</sup>

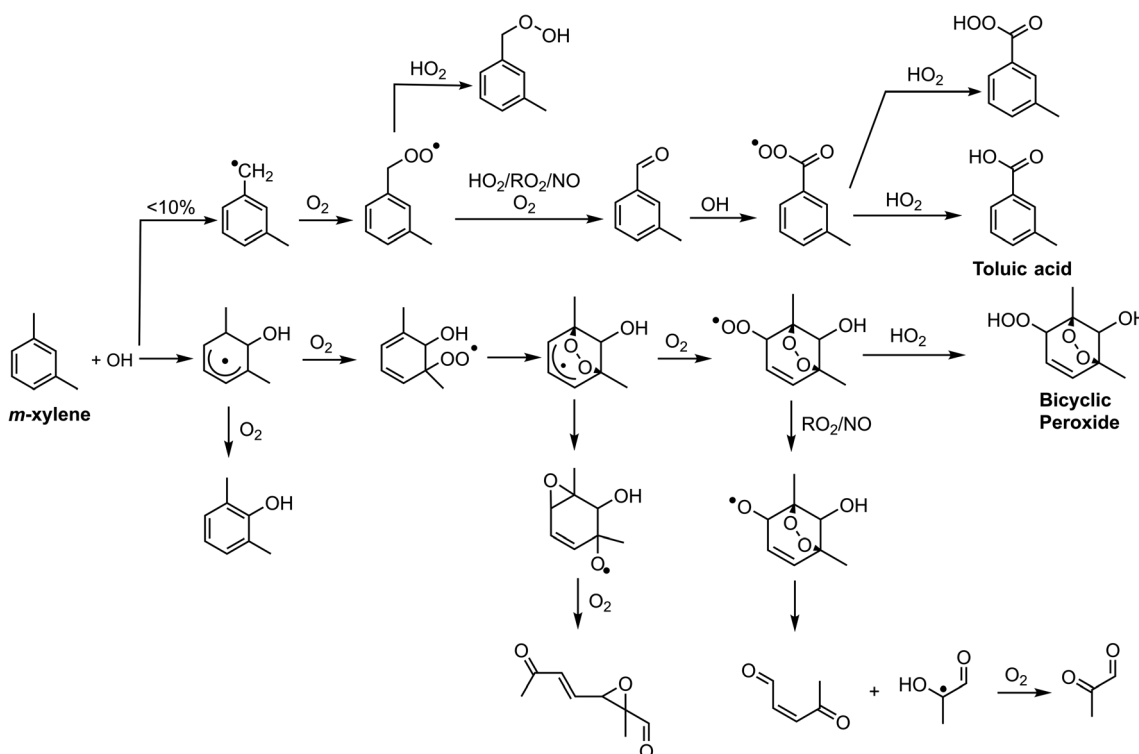
Scheme 2 Selected oxidation pathways for *m*-xylene + OH.

Fig. 2a–c plots 2-methyl-1,4-benzoquinone, the bicyclic peroxide and *m*-toluic acid for  $\text{Cl}_2$ ,  $\text{ClNO}_2$ , and  $\text{H}_2\text{O}_2$  experiments. Growth of 2-methyl-1,4-benzoquinone is only substantial when  $\text{Cl}_2$  is present, including under high  $\text{NO}_x$  conditions (Fig. S2†), indicating that high Cl radical concentrations initiate this multigenerational chemistry. Greater relative formation of 2-methyl-1,4-benzoquinone over *m*-toluic acid and bicyclic peroxide occurred in both low  $\text{NO}_x$   $\text{Cl}_2$  experiments (Exp. 4 and 5). According to our chamber box model (Fig. S10†), integrated Cl radical exposures during the full UV exposure period are  $8 \times 10^9$  molecules per  $\text{cm}^3$  per s and  $14 \times 10^9$  molecules per  $\text{cm}^3$  per s under high and low  $\text{NO}_x$  conditions, respectively. In contrast, little growth of the quinone product is observed in a  $\text{ClNO}_2$  experiment with modeled Cl radical exposure of  $5 \times 10^9$  molecules per  $\text{cm}^3$  per s. In addition, model results (Fig. S10†) indicate  $\text{Cl}_2$  generates peak Cl radical concentrations nearly 1 order of magnitude higher than  $\text{ClNO}_2$  as a result of the high  $\text{Cl}_2$  photolysis rate. Increased Cl radical concentrations may offer more opportunity for multiple radical oxidation events which drive formation of the quinone product. This mirrors previously observed differences in SOA formation from high  $\text{NO}_x$  *m*-xylene + OH systems.<sup>10</sup> In this prior work, use of photolabile HONO produced a rapid plume of OH radicals which generated SOA not observed in classical high  $\text{NO}_x$  photooxidation experiments which rely on  $\text{NO}_x$  and  $\text{HO}_x$  cycling to generate OH radicals more slowly. Higher radical concentrations reduce the timescale of multigenerational chemistry and lower SVOCs wall losses in addition to potentially altering radical fate branching pathways.<sup>10</sup>

However, we observe continued formation of 2-methyl-1,4-benzoquinone in  $\text{Cl}_2 + \text{NO}$  experiments even after Cl radical concentrations fall below those observed in  $\text{ClNO}_2$  experiments (Fig. S2 and S10†). This is likely related to differences in initial  $\text{RO}_2$  radical fate which drive precursor availability. High initial Cl radical concentrations combined with the presence of NO bias  $\text{Cl}_2 + \text{NO}$  oxidation environments toward  $\text{RO}_2 + \text{NO}$  radical terminations or shift the fate of the Criegee intermediate toward reaction with Cl to form methyl benzaldehyde. Formation of these key precursors is suppressed in the  $\text{ClNO}_2$  case due to slower formation of NO and higher OH to Cl ratio which drives  $\text{HO}_2$  formation and efficient formation of the bicyclic peroxide radical. The presence of benzaldehyde and other precursors in  $\text{Cl}_2 + \text{NO}$  experiments enables formation of the benzoquinone products even as the OH to Cl ratio increases.

Bicyclic peroxide product formation is observed for all experiments except the low  $\text{NO}_x$   $\text{Cl}_2$  case. Unsurprisingly, hydrogen peroxide experiments rapidly generated this OH oxidation product. Chlorine gas in the absence of  $\text{NO}_x$  formed minimal secondary OH radicals with an OH radical exposure of  $1.5 \times 10^9$  molecules per  $\text{cm}^3$  per s. In contrast,  $\text{Cl}_2 + \text{NO}$  and  $\text{ClNO}_2$  experiments have OH radical exposures of 43 and  $35 \times 10^9$  molecules per  $\text{cm}^3$  per s, respectively. This  $\text{NO}_x$  enhancement of hydroxyl radicals is driven both by the effect of OH regeneration through  $\text{NO}_x$  cycling and the presence of secondary OH formation pathways which are enhanced by  $\text{NO}_x$  reaction with peroxy radicals.<sup>39</sup> The formation of bicyclic peroxides in the  $\text{ClNO}_2$  case was more rapid than in the  $\text{Cl}_2 + \text{NO}$

case (Fig. S2†) and was observed in both  $\text{ClNO}_2$  experiments (Exp. 1 and 2). Under both conditions, similar OH radical concentrations/exposures are achieved (Fig. S10†); however, slower formation of Cl radicals from  $\text{ClNO}_2$  likely biases initial oxidation toward OH radical addition pathways compared to initial Cl oxidations in the  $\text{Cl}_2 + \text{NO}$  case. As discussed, peak Cl radical concentrations in the  $\text{Cl}_2 + \text{NO}$  case result in multigenerational Cl chemistry. The reduced Cl concentration in the nitryl chloride system generated an approximate 1 : 10 Cl : OH radical ratio, similar to ambient measurements of a 1 to 2 order of magnitude difference in Cl and OH radical concentrations in inland Texas.<sup>28</sup> In the case of  $\text{Cl}_2 + \text{NO}$ , we observe a shifting Cl : OH radical ratio of 1 : 2 initially to nearly 1 : 50 during hour-long photo-oxidation. In addition, dark chemistry is observed following photooxidation in the  $\text{ClNO}_2$  experiment, as evidenced by growth in nitryl chloride and a decline in *m*-toluic acid. This may be related to heterogeneous chemistry which forms nitryl chloride from  $\text{N}_2\text{O}_5$  interactions with chloride containing particles. We do see growth of  $\text{N}_2\text{O}_5$  in the dark for  $\text{ClNO}_2$  experiments (Fig. S6†), possibly from reaction of  $\text{NO}_2$  and  $\text{NO}_3$  in the gas phase which goes on to react with chloride and form nocturnal  $\text{ClNO}_2$ . This behavior is not observed when  $\text{ClNO}_2$  is used in combination with  $\text{Cl}_2$  and/or  $\text{H}_2\text{O}_2$  (Exp. 8 and 10, Fig. S3 and S4†), likely due to lower availability of  $\text{N}_2\text{O}_5$  precursors. Taken together, these results indicate that oxidative environments from fresh chlorine emissions in high  $\text{NO}_x$  areas differ from  $\text{ClNO}_2$  rich air masses typically observed in the early morning.

*m*-Toluic acid is observed to form during photo-oxidation in all experiments. Formation of toluic acid is substantially lower in  $\text{H}_2\text{O}_2$  experiments, consistent with the OH oxidation pathway which favors ring addition over hydrogen abstraction. Under high  $\text{NO}_x$   $\text{Cl}_2$  conditions (Fig. S2†), formation of toluic acid is more rapid than 2-methyl-1,4-benzoquinone. This may indicate termination of radical propagation is more rapid under high  $\text{NO}_x$  conditions or may be a result of additional competition for the Cl radical as it forms  $\text{ClNO}$ ,  $\text{ClONO}$ , and  $\text{ClNO}_2$  in the presence of  $\text{NO}_x$ .

In addition to these species, organochlorine species are formed in chlorine radical systems. Gas phase organochlorine fraction was calculated by dividing the total  $\text{C}_{2-10}\text{H}_y\text{O}_z\text{Cl}_{1-3}\text{I}^-$  signal by the total  $\text{C}_{1-10}\text{I}^-$  signal (*i.e.* total organic species signal) averaged for 10 minutes following the end of UV photolysis. We assume a uniform sensitivity for all organic species. Under low  $\text{NO}_x$  conditions, we find a gas phase organochlorine fraction of 0.22 which falls to 0.18 under  $\text{Cl}_2 + \text{NO}$  and falls further to 0.07 when  $\text{ClNO}_2$  is used. This is consistent with the growth in OH radical concentrations observed from  $\text{Cl}_2$  to  $\text{Cl}_2 + \text{NO}$  to  $\text{ClNO}_2$  experiments. These gas phase chlorinated species are a result of chlorine addition reactions, likely to available double bonds following aromatic ring breaking.

### 3.2 Chlorine oxidation yields more highly oxidized SOA

Differences in gas phase oxidation discussed above lead to differences in particle phase composition. Fig. 3 shows

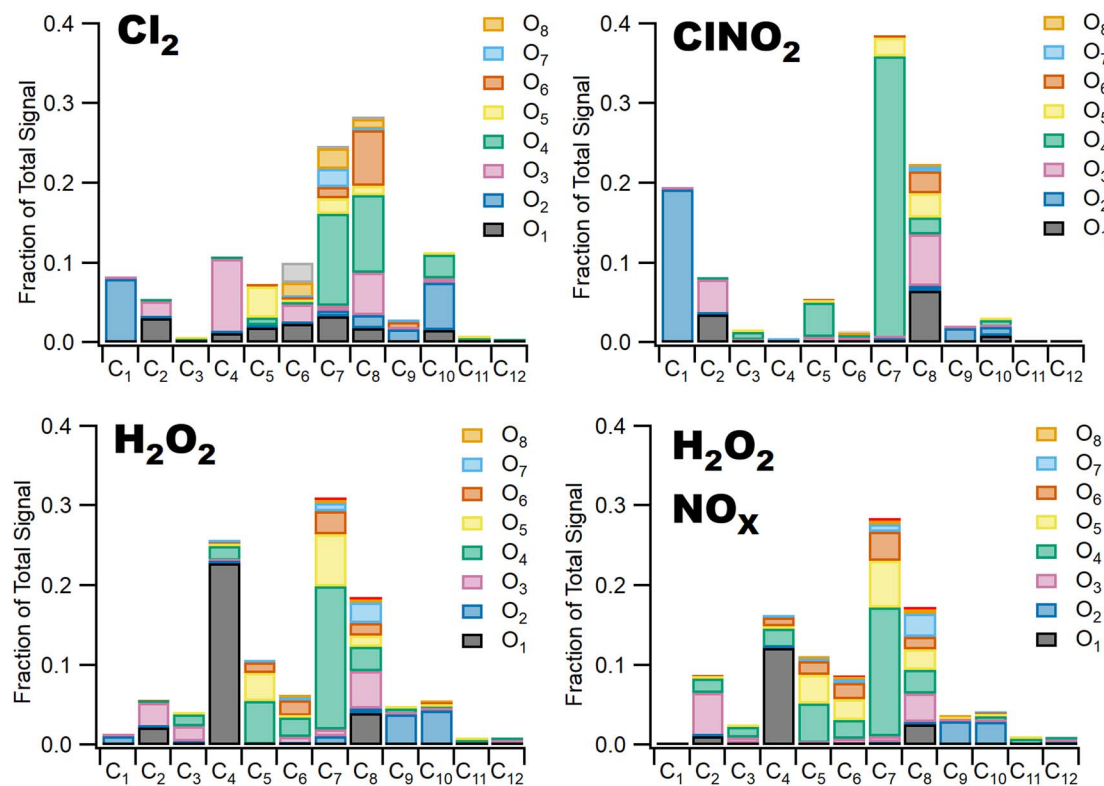


Fig. 3  $\text{I}^-$  FIGAERO-CIMS desorption data from experiment 1 ( $\text{ClNO}_2$ ), 4 ( $\text{Cl}_2$ ), 6 ( $\text{H}_2\text{O}_2 + \text{NO}_x$ ) and 7 ( $\text{H}_2\text{O}_2$ ). Particle phase species are categorized by carbon and oxygen number, integrated over their desorption curves, summed and divided by total integrated desorption signal of represented species.

integrated particle composition data from the FIGAERO-CIMS from experiments 1, 4, 6, and 7. Particles were collected for 45 minutes following the end of UV exposure and desorbed on a 45 minutes heating cycle. Integration of the thermal desorption signal is performed over the full desorption temperature range (25–180 °C). Experiments using  $\text{Cl}_2$  as radical precursor resulted in more highly oxidized organic aerosol; for example, the experiments formed a higher fraction of  $\text{C}_{7-8}\text{O}_{4-8}$  species compared to experiments using  $\text{ClNO}_2$  which formed a much smaller fraction of species with more than four oxygen atoms. This additional oxygen content may be related to the more rapid formation of Cl radicals under  $\text{Cl}_2$  oxidation conditions, driving multigenerational oxidation chemistry. In addition, the fraction of ring retaining  $\text{C}_8$  species is higher in SOA formed when  $\text{Cl}_2$  was used as the radical precursor, consistent with functionalization of the methyl group after hydrogen abstraction. SOA formed in experiments where  $\text{ClNO}_2$  or  $\text{H}_2\text{O}_2$  serves as the radical precursor has a higher fraction of  $\text{C}_7$  species. Even greater fragmentation to  $\text{C}_4$  and  $\text{C}_5$  species is observed in hydrogen peroxide experiments, consistent with the ring breaking fragmentation products resulting from the bicyclic radicals formed by OH ring addition chemistry.

These observations are consistent with bulk particle composition from the ACSM. Triangle plot analysis<sup>54</sup> (Fig. 4) shows that the fraction of the total organic signal due to organic mass at  $m/z$  44 ( $f_{44}$ ) was elevated and  $f_{43}$  was reduced in  $\text{Cl}_2$  experiments. This indicated use of pure  $\text{Cl}_2$  as a radical

precursor resulted in more highly oxidized SOA with increased formation of acid groups. Use of  $\text{ClNO}_2$  resulted in similar  $f_{44}$  fractions to  $\text{H}_2\text{O}_2$  experiments. In addition,  $f_{43}$  fractions were higher in  $\text{H}_2\text{O}_2$  experiments, indicating that less oxidized SOA was the norm when primary OH radicals are present. This is consistent with observations of toluene + Cl and toluene + OH chemistry from Dhulipala *et al.* (2019)<sup>22</sup> where toluene + Cl SOA had a lower  $f_{43}$  and higher  $f_{44}$  measured in the ACSM than toluene + OH SOA. This was attributed to formation of ring opened products from OH oxidation with unoxidized methyl groups related to higher  $f_{43}$  values. SOA from *m*-xylene +  $\text{H}_2\text{O}_2$  experiments in Loza *et al.* (2011)<sup>55</sup> resulted in higher  $f_{43}$  values measured in the aerosol mass spectrometer (AMS) than reported here, though  $f_{44}$  values are similar.

Particle phase organochlorine content varied with radical precursor as shown by the ratio of  $\text{HCl}^+$  ( $m/z$  36) to organics in the ACSM. ACSM  $\text{HCl}^+$  to organics ratio has been suggested as an improved semi-quantitative measure of particulate organochlorine compared to the detection utilizing  $\text{Cl}^+$  ( $m/z$  35).<sup>24</sup> Here, we found that the  $\text{HCl}^+$  to organics ratio decreased from 0.037 in a  $\text{Cl}_2$  experiment to 0.025 and 0.011 in  $\text{Cl}_2 + \text{NO}$  and  $\text{ClNO}_2$  experiments, respectively. FIGAERO-CIMS particle desorption signals show that in  $\text{Cl}_2$  experiments organochlorine species make up 0.27 of total identified desorption signal. This falls to 0.07 for  $\text{ClNO}_2$  experiments. This behavior is qualitatively consistent with gas phase decreases in organochlorine content



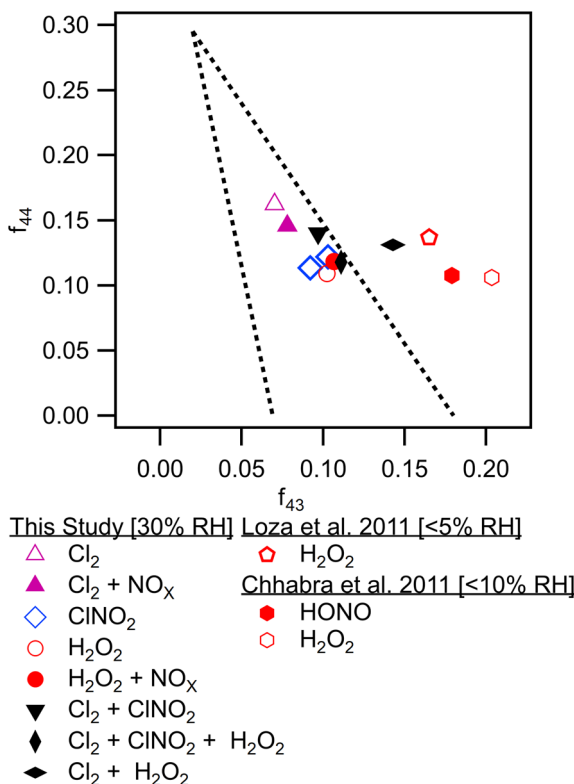


**Fig. 4**  $f_{44}$  to  $f_{43}$  triangle plot for all chamber experiments from final average ACSM bulk particle composition. Data from literature sources is shown.<sup>46,47</sup>

discussed earlier. The behavior is also qualitatively consistent with the ACSM HCl/Organics ratio.

While  $\text{NO}_x$  resulted in less oxidized SOA in  $\text{Cl}_2$  experiments, it had little effect within peroxide experiments. This may be driven by  $\text{H}_2\text{O}_2$  photolysis generating substantial  $\text{HO}_2$  and favoring  $\text{HO}_2 + \text{RO}_2$  and  $\text{RO}_2 + \text{RO}_2$  chemistry over  $\text{NO}_x + \text{RO}_2$  pathways. Use of  $\text{HONO}$  as a high  $\text{NO}_x$  source of OH radicals promoted a more substantial shift in SOA oxidation state compared to  $\text{H}_2\text{O}_2$  for *m*-xylene oxidation in Chhabra *et al.* (2011).<sup>56</sup> This may be because the photolysis of  $\text{HONO}$  produces a lower  $\text{HO}_2$  to  $\text{RO}_2$  ratio as well as higher initial OH radical concentrations. The  $f_{43}/f_{44}$  differences in this study compared to literature may be related to instrument variability as noted in Ng *et al.* (2010).<sup>54</sup> Differences in  $f_{43}/f_{44}$  may also be driven by increased humidity as discussed in Zhang *et al.* (2019),<sup>13</sup> where a shift in O:C ratio was observed for *m*-xylene + OH experiments. The higher RH in these experiments may reduce the degree of oxidation observed in the particle phase by reducing the formation of low-volatility oligomers. This effect has also been reported in toluene<sup>57</sup> and isoprene<sup>58</sup> studies.

### 3.3 Oxidant environment shifts SOA formation

In addition to SOA composition, SOA formation and yield is also dependent on radical precursor choice. Table 1 lists peak wall loss corrected SOA concentrations. Peak SOA formation is greatest for the low NO<sub>x</sub> Cl<sub>2</sub> condition (experiment 4) compared

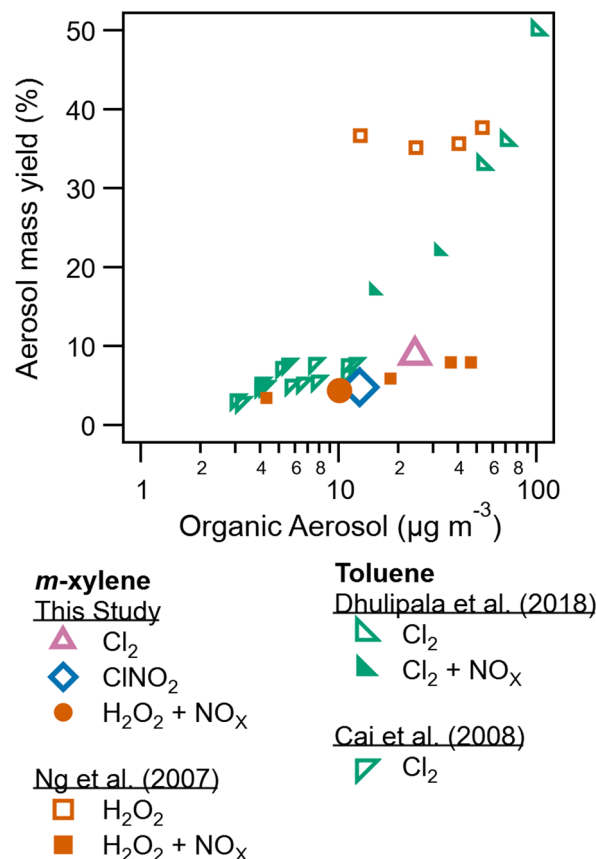


**Fig. 5** Aerosol mass yield plotted against organic aerosol concentration from this study, Ng *et al.* (2007),<sup>10</sup> Dhulipala *et al.* (2018),<sup>33</sup> and Cai *et al.* (2008).<sup>23</sup> This study and Ng *et al.* (2007)<sup>10</sup> utilize *m*-xylene while the other studies utilize toluene. Data from this study are shown in larger symbols for emphasis.

to SOA formation for  $\text{ClNO}_2$  (experiment 2) and high  $\text{NO}_x$   $\text{Cl}_2$  (experiment 3). This reduction in SOA formation due to  $\text{NO}_x$  has been previously reported for some aromatic and hydroxyl radical systems.<sup>10</sup> Peroxy radical fate drives these differences, with  $\text{NO} + \text{RO}_2$  pathways resulting in more volatile products compared to  $\text{HO}_2 + \text{RO}_2$  reaction products.<sup>9</sup>

Secondary organic aerosol yields are determined as the mass concentration of SOA formed divided by the mass concentration of precursor consumed. Yields are reported for experiments 2, 4, and 6, the three experiments were measurements of *m*-xylene consumption were available based on  $\text{H}_3\text{O}^+$  CIMS measurements. Measured and modeled *m*-xylene consumption is shown in Fig. S7–S9.† Fig. 5 compares yields from this study to literature. The highest yield (8.8%) is observed for the low  $\text{NO}_x$   $\text{Cl}_2$  condition. Yield for the *m*-xylene +  $\text{ClNO}_2$  system was found to be 4.8% here. While yields for the *m*-xylene + Cl reaction has not been previously reported, toluene +  $\text{Cl}_2$  experiments report yields as low as 5% (ref. 23) and as high at 82%.<sup>22</sup> Toluene and *m*-xylene are similar molecules, though the additional methyl group on *m*-xylene may alter the volatility of expected product by providing an additional site for Cl hydrogen abstraction. In addition, previous studies differ substantially in use of seed aerosol, relative humidity, and  $\text{Cl}_2/\text{VOC}$  ratio from this one.

Prior studies have observed a substantial dependence of SOA formation from Cl radicals on Cl<sub>2</sub>/VOC ratio.<sup>23,53</sup>

For the high NO<sub>x</sub> H<sub>2</sub>O<sub>2</sub> system, yields agree with those presented in Ng *et al.* (2007).<sup>10</sup> Substantially higher formation and yield is observed in Ng *et al.* (2007) for low NO<sub>x</sub> conditions, though differences in humidity between these experiments and the one described there may play a role. Zhang *et al.* (2019)<sup>13</sup> show a sharp drop in SOA yield with increasing RH, related to increased wall losses of semi volatile species and reduced oligomerization as previously discussed.

## 4 Conclusions

This environmental chamber study examined the impact of radical precursor identity on Cl and OH oxidation of *m*-xylene. Hydrogen peroxide experiments resulted in well studied hydroxyl radical chemistry which primarily leads to bicyclic radical formation and subsequent fragmentation due to OH ring addition. Chlorine gas used as a Cl precursor drove rapid oxidation by hydrogen abstraction from methyl substituents and addition of oxygenated functional groups. In addition, chlorine gas drove the formation of a multigenerational product (2-methyl-1,4-benzoquinone) under both high and low NO<sub>x</sub> conditions. In contrast, nitryl chloride generated a different high NO<sub>x</sub> Cl radical environment which did not form 2-methyl-1,4-benzoquinone. Furthermore, the formation of secondary hydroxyl radicals is substantial and results in formation of bicyclic radical species in high NO<sub>x</sub> Cl radical environments. In ambient air masses with high concentrations of chlorine gas, including marine regions or certain industrial plumes, functionalized aromatics and toxic compounds including quinones and organochlorine species will be rapidly formed. In those ambient early morning air masses with high nitryl chloride concentrations, greater fragmentation of aromatic hydrocarbons is anticipated with reduced formation of organochlorine species as secondary OH radicals dominate oxidation. Broadly, differences in chlorine radical exposure, peak chlorine radical concentrations, and formation of secondary hydroxyl radicals all drive different chemical outcomes for environments dominated by fresh chlorine gas in the presence of NO<sub>x</sub> compared to those dominated by nitryl chloride.

In the particle phase, Cl<sub>2</sub> drove less fragmentation and greater functionalization of organic species than H<sub>2</sub>O<sub>2</sub> consistent with previous observations of toluene + Cl/OH chemistry. Reduced fragmentation was also observed when ClNO<sub>2</sub> was used, though chlorine gas generated more highly oxidized aerosol. This is consistent with gas phase oxidation pathways described above as OH ring addition chemistry leads to the fragmentation of the bicyclic radical intermediate. Consistent with rates and degrees of precursor consumption, SOA mass formed under low NO<sub>x</sub> Cl<sub>2</sub> conditions was greatest, while the presence of NO<sub>x</sub> suppressed formation and yield as seen in other studies. Despite the high secondary hydroxyl radical formation observed in Cl radical experiments, the composition of organic aerosol from Cl<sub>2</sub> and ClNO<sub>2</sub> differs substantially from OH oxidation alone. Atmospherically, the reduced fragmentation and increased functionalization of particle phase

aromatics following Cl oxidation may substantially alter SOA properties. Functionalized aromatics may act as chromophores which alter aerosol light absorption, while organochlorine species may be toxic. Furthermore, organochlorine species in the aerosol phase may contribute to heterogenous reactions that regenerate Cl<sub>2</sub> and ClNO<sub>2</sub>. Accounting for the particle phase differences resulting from Cl oxidation compared to OH oxidation is necessary to fully capture climate and health impacts.

Oxidation of aromatic hydrocarbons and subsequent SOA formation may have substantial impacts on tropospheric pollution. As shown here, Cl<sub>2</sub> and ClNO<sub>2</sub> generate substantially different radical environments and subsequently form different product mixtures. Radical precursor identity and the resulting oxidative environment demands future study in both laboratory and field measurement settings. With growing evidence of high particulate chloride in polluted megacities and the evolution of chlorine radical precursors from industrial and mineral sources, there is a premium on better understanding and constraining the fate and transport of chlorine in the environment.

## Data availability

Experimental data are available in the ICARUS database. Data published in the main manuscript's figures are available *via* the Texas Data Repository <https://doi.org/10.18738/T8/6XWHN9>. Underlying research data are also available by request to Lea Hildebrandt Ruiz (lhr@che.utexas.edu).

## Author contributions

Nirvan Bhattacharyya: conceptualization, methodology, investigation, formal analysis, writing – original draft. Mrinali Modi: software, formal analysis, writing – review & editing. Leif G. Jahn: writing – review & editing. Lea Hildebrandt Ruiz: conceptualization, supervision, funding acquisition, writing – review & editing.

## Conflicts of interest

The authors declare no conflicts of interest.

## Acknowledgements

The authors would like to acknowledge the support of staff at the Center for Engineering and Environmental Resources including Denzil Smith, Susan McCoy and Nohemi Cazares in building management, ordering, and other logistics. The authors are also grateful for funding support from the National Science Foundation (Grant number 1653625) and the Welch Foundation (Grant numbers F-1925-20170325 and F-1925-20200401).

## References

- 1 G. Huang, R. Brook, M. Crippa, G. Janssens-Maenhout, C. Schieberle, C. Dore, D. Guizzardi, M. Muntean,

E. Schaaf and R. Friedrich, Speciation of anthropogenic emissions of non-methane volatile organic compounds: a global gridded data set for 1970–2012, *Atmos. Chem. Phys.*, 2017, **17**, 7683–7701.

2 T. Salameh, S. Sauvage, C. Afif, A. Borbon and N. Locoge, Source apportionment vs. emission inventories of non-methane hydrocarbons (NMHC) in an urban area of the Middle East: local and global perspectives, *Atmos. Chem. Phys.*, 2016, **16**, 3595–3607.

3 J. An, Y. Huang, C. Huang, X. Wang, R. Yan, Q. Wang, H. Wang, S. Jing, Y. Zhang, Y. Liu, Y. Chen, C. Xu, L. Qiao, M. Zhou, S. Zhu, Q. Hu, J. Lu and C. Chen, Emission inventory of air pollutants and chemical speciation for specific anthropogenic sources based on local measurements in the Yangtze River Delta region, China, *Atmos. Chem. Phys.*, 2021, **21**, 2003–2025.

4 R. R. Hoque, P. S. Khillare, T. Agarwal, V. Shridhar and S. Balachandran, Spatial and temporal variation of BTEX in the urban atmosphere of Delhi, India, *Sci. Total Environ.*, 2008, **392**, 30–40.

5 S. C. Lee, M. Y. Chiu, K. F. Ho, S. C. Zou and X. Wang, Volatile organic compounds (VOCs) in urban atmosphere of Hong Kong, *Chemosphere*, 2002, **48**, 375–382.

6 J. Zhao, R. Zhang, K. Misawa and K. Shibuya, Experimental product study of the OH-initiated oxidation of m-xylene, *J. Photochem. Photobiol. A*, 2005, **176**, 199–207.

7 R. Atkinson and J. Arey, Mechanisms of the gas-phase reactions of aromatic hydrocarbons and PAHS with OH and NO<sub>3</sub> radicals, *Polycyclic Aromat. Compd.*, 2007, **27**, 15–40.

8 M. Wang, D. Chen, M. Xiao, Q. Ye, D. Stolzenburg, V. Hofbauer, P. Ye, A. L. Vogel, R. L. Mauldin, A. Amorim, A. Baccarini, B. Baumgartner, S. Brilke, L. Dada, A. Dias, J. Duplissy, H. Finkenzeller, O. Garmash, X. C. He, C. R. Hoyle, C. Kim, A. Kvashnin, K. Lehtipalo, L. Fischer, U. Molteni, T. Petäjä, V. Pospisilova, L. L. J. Quéléver, M. Rissanen, M. Simon, C. Tauber, A. Tomé, A. C. Wagner, L. Weitz, R. Volkamer, P. M. Winkler, J. Kirkby, D. R. Worsnop, M. Kulmala, U. Baltensperger, J. Dommen, I. El-Haddad and N. M. Donahue, Photo-oxidation of Aromatic Hydrocarbons Produces Low-Volatility Organic Compounds, *Environ. Sci. Technol.*, 2020, **54**, 7911–7921.

9 D. K. Henze, J. H. Seinfeld, N. L. Ng, J. H. Kroll, T. M. Fu, D. J. Jacob and C. L. Heald, Global modeling of secondary organic aerosol formation from aromatic hydrocarbons: high- vs. low-yield pathways, *Atmos. Chem. Phys.*, 2008, **8**, 2405–2421.

10 N. L. Ng, J. H. Kroll, A. W. H. Chan, P. S. Chhabra, R. C. Flagan and J. H. Seinfeld, Secondary organic aerosol formation from m-xylene, toluene, and benzene, *Atmos. Chem. Phys.*, 2007, **7**, 3909–3922.

11 C. G. Fletcher, B. Kravitz and B. Badawy, Quantifying uncertainty from aerosol and atmospheric parameters and their impact on climate sensitivity, *Atmos. Chem. Phys.*, 2018, **18**, 17529–17543.

12 M. Brauer, G. Freedman, J. Frostad, A. van Donkelaar, R. V. Martin, F. Dentener, R. van Dingenen, K. Estep, H. Amini, J. S. Apte, K. Balakrishnan, L. Barregard, D. Broday, V. Feigin, S. Ghosh, P. K. Hopke, L. D. Knibbs, Y. Kokubo, Y. Liu, S. Ma, L. Morawska, J. L. T. Sangrador, G. Shaddick, H. R. Anderson, T. Vos, M. H. Forouzanfar, R. T. Burnett and A. Cohen, Ambient Air Pollution Exposure Estimation for the Global Burden of Disease 2013, *Environ. Sci. Technol.*, 2016, **50**, 79–88.

13 Q. Zhang, Y. Xu and L. Jia, Secondary organic aerosol formation from OH-initiated oxidation of m-xylene: effects of relative humidity on yield and chemical composition, *Atmos. Chem. Phys.*, 2019, **19**, 15007–15021.

14 C. Song, K. Na, B. Warren, Q. Malloy and D. R. Cocker, Secondary organic aerosol formation from m-xylene in the absence of NO<sub>x</sub>, *Environ. Sci. Technol.*, 2007, **41**, 7409–7416.

15 L. Hildebrandt, N. M. Donahue and S. N. Pandis, High formation of secondary organic aerosol from the photo-oxidation of toluene, *Atmos. Chem. Phys.*, 2009, **9**, 2973–2986.

16 X. Wang, D. J. Jacob, S. D. Eastham, M. P. Sulprizio, L. Zhu, Q. Chen, B. Alexander, T. Sherwen, M. J. Evans, B. H. Lee, J. D. Haskins, F. D. Lopez-Hilfiker, J. A. Thornton, G. L. Huey and H. Liao, The role of chlorine in global tropospheric chemistry, *Atmos. Chem. Phys.*, 2019, **19**, 3981–4003.

17 L. Wang, J. Arey and R. Atkinson, Reactions of chlorine atoms with a series of aromatic hydrocarbons, *Environ. Sci. Technol.*, 2005, **39**, 5302–5310.

18 T. P. Riedel, T. H. Bertram, T. A. Crisp, E. J. Williams, B. M. Lerner, A. Vlasenko, S.-M. Li, J. Gilman, J. de Gouw, D. M. Bon, N. L. Wagner, S. S. Brown and J. A. Thornton, Nitryl Chloride and Molecular Chlorine in the Coastal Marine Boundary Layer, *Environ. Sci. Technol.*, 2012, **46**, 10463–10470.

19 A. W. H. Chan, J. H. Kroll, N. L. Ng and J. H. Seinfeld, Kinetic modeling of secondary organic aerosol formation: effects of particle-and gas-phase reactions of semivolatile products, *Atmos. Chem. Phys.*, 2007, **7**, 4135–4147.

20 J. Fan and R. Zhang, Density functional theory study on OH-initiated atmospheric oxidation of m-xylene, *J. Phys. Chem. A*, 2008, **112**, 4314–4323.

21 P. J. Ziemann and R. Atkinson, Kinetics, products, and mechanisms of secondary organic aerosol formation, *Chem. Soc. Rev.*, 2012, **41**, 6582–6605.

22 S. V. Dhulipala, S. Bhandari and L. Hildebrandt Ruiz, Formation of oxidized organic compounds from Cl-initiated oxidation of toluene, *Atmos. Environ.*, 2019, **199**, 265–273.

23 X. Cai, L. D. Ziembra and R. J. Griffin, Secondary aerosol formation from the oxidation of toluene by chlorine atoms, *Atmos. Environ.*, 2008, **42**, 7348–7359.

24 D. S. Wang and L. Hildebrandt Ruiz, Secondary organic aerosol from chlorine-initiated oxidation of isoprene, *Atmos. Chem. Phys.*, 2017, **17**, 13491–13508.

25 D. S. Wang and L. Hildebrandt Ruiz, Chlorine-initiated oxidation of n-alkanes under high-NO<sub>x</sub> conditions: insights into secondary organic aerosol composition and volatility using a FIGAERO-CIMS, *Atmos. Chem. Phys.*, 2018, **18**, 15535–15553.



26 C. G. Masoud and L. Hildebrandt Ruiz, Chlorine-Initiated Oxidation of  $\alpha$ -Pinene: Formation of Secondary Organic Aerosol and Highly Oxygenated Organic Molecules, *ACS Earth Space Chem.*, 2021, **5**, 2307–2319.

27 P. L. Tanaka, S. Oldfield, J. D. Neece, C. B. Mullins and D. T. Allen, Anthropogenic sources of chlorine and ozone formation in urban atmospheres, *Environ. Sci. Technol.*, 2000, **34**, 4470–4473.

28 C. B. Faxon, J. Bean and L. Hildebrandt Ruiz, Inland Concentrations of  $\text{Cl}_2$  and  $\text{ClNO}_2$  in Southeast Texas Suggest Chlorine Chemistry Significantly Contributes to Atmospheric Reactivity, *Atmosphere*, 2015, **6**, 1487–1506.

29 H. D. Osthoff, J. M. Roberts, A. R. Ravishankara, E. J. Williams, B. M. Lerner, R. Sommariva, T. S. Bates, D. Coffman, P. K. Quinn, J. E. Dibb, H. Stark, J. B. Burkholder, R. K. Talukdar, J. Meagher, F. C. Fehsenfeld and S. S. Brown, High levels of nitryl chloride in the polluted subtropical marine boundary layer, *Nat. Geosci.*, 2008, **1**, 324–328.

30 G. J. Phillips, M. J. Tang, J. Thieser, B. Brickwedde, G. Schuster, B. Bohn, J. Lelieveld and J. N. Crowley, Significant concentrations of nitryl chloride observed in rural continental Europe associated with the influence of sea salt chloride and anthropogenic emissions, *Geophys. Res. Lett.*, 2012, **9**(10), L10811.

31 C. Masoud, M. Modi, N. Bhattacharyya, L. Jahn, K. McPherson, P. Abue, K. Patel, D. Allen and L. Hildebrandt Ruiz, High chlorine concentrations in an unconventional oil and gas development region and impacts on atmospheric chemistry, *Environ. Sci. Technol. Lett.*, 2023, (Submitted).

32 C. B. Faxon and D. T. Allen, Chlorine chemistry in urban atmospheres: a review, *Environ. Chem.*, 2013, **10**, 221–233.

33 C. B. Faxon, S. V. Dhulipala, D. T. Allen and L. Hildebrandt Ruiz, Heterogeneous production of  $\text{Cl}_2$  from particulate chloride: effects of composition and relative humidity, *AIChE J.*, 2018, **64**, 3151–3158.

34 A. T. Ahern, L. Goldberger, L. Jahl, J. Thornton and R. C. Sullivan, Production of  $\text{N}_2\text{O}_5$  and  $\text{ClNO}_2$  through Nocturnal Processing of Biomass-Burning Aerosol, *Environ. Sci. Technol.*, 2018, **52**, 550–559.

35 S. M. McNamara, Q. Chen, J. Edebeli, K. D. Kulju, J. Mumpfield, J. D. Fuentes, S. B. Bertman and K. A. Pratt, Observation of  $\text{N}_2\text{O}_5$  Deposition and  $\text{ClNO}_2$  Production on the Saline Snowpack, *ACS Earth Space Chem.*, 2021, **5**, 1020–1031.

36 D. Mitroo, T. E. Gill, S. Haas, K. A. Pratt and C. J. Gaston,  $\text{ClNO}_2$  Production from  $\text{N}_2\text{O}_5$  Uptake on Saline Playa Dusts: New Insights into Potential Inland Sources of  $\text{ClNO}_2$ , *Environ. Sci. Technol.*, 2019, **53**, 7442–7452.

37 S. Gani, S. Bhandari, S. Seraj, D. S. Wang, K. Patel, P. Soni, Z. Arub, G. Habib, L. Hildebrandt Ruiz and J. S. Apte, Submicron aerosol composition in the world's most polluted megacity: the Delhi Aerosol Supersite study, *Atmos. Chem. Phys.*, 2019, **19**, 6843–6859.

38 R. Atkinson, Gas-phase tropospheric chemistry of organic compounds: a review, *Atmos. Environ.*, 2007, **41**, 200–240.

39 C. J. Young, R. A. Washenfelder, P. M. Edwards, D. D. Parrish, J. B. Gilman, W. C. Kuster, L. H. Mielke, H. D. Osthoff, C. Tsai, O. Pikelnaya, J. Stutz, P. R. Veres, J. M. Roberts, S. Griffith, S. Dusanter, P. S. Stevens, J. Flynn, N. Grossberg, B. Lefer, J. S. Holloway, J. Peischl, T. B. Ryerson, E. L. Atlas, D. R. Blake and S. S. Brown, Chlorine as a primary radical: evaluation of methods to understand its role in initiation of oxidative cycles, *Atmos. Chem. Phys.*, 2014, **14**, 3427–3440.

40 C. Song, K. Na and D. R. Cocker, Impact of the hydrocarbon to  $\text{NO}_x$  ratio on secondary organic aerosol formation, *Environ. Sci. Technol.*, 2005, **39**, 3143–3149.

41 R. D. Thaler, L. H. Mielke and H. D. Osthoff, Quantification of Nitryl Chloride at Part Per Trillion Mixing Ratios by Thermal Dissociation Cavity Ring-Down Spectroscopy, *Anal. Chem.*, 2011, **83**, 2761–2766.

42 N. L. Ng, S. C. Herndon, A. Trimborn, M. R. Canagaratna, P. L. Croteau, T. B. Onasch, D. Sueper, D. R. Worsnop, Q. Zhang, Y. L. Sun and J. T. Jayne, An Aerosol Chemical Speciation Monitor (ACSM) for Routine Monitoring of the Composition and Mass Concentrations of Ambient Aerosol, *Aerosol Sci. Technol.*, 2011, **45**, 780–794.

43 B. H. Lee, F. D. Lopez-Hilfiker, C. Mohr, T. K. Kurtén, D. R. Worsnop and J. A. Thornton, An Iodide-Adduct High-Resolution Time-of-Flight Chemical-Ionization Mass Spectrometer: Application to Atmospheric Inorganic and Organic Compounds, *Environ. Sci. Technol.*, 2014, **48**, 6309–6317.

44 F. D. Lopez-Hilfiker, C. Mohr, M. Ehn, F. Rubach, E. Kleist, J. Wildt, T. F. Mentel, A. Lutz, M. Hallquist, D. Worsnop and J. A. Thornton, A novel method for online analysis of gas and particle composition: description and evaluation of a Filter Inlet for Gases and AEROSols (FIGAERO), *Atmos. Meas. Tech.*, 2014, **7**, 983–1001.

45 W. P. L. Carter, Development of a condensed SAPRC-07 chemical mechanism, *Atmos. Environ.*, 2010, **44**, 5336–5345.

46 P. L. Tanaka, D. T. Allen, E. C. McDonald-Buller, S. Chang, Y. Kimura, C. B. Mullins, G. Yarwood and J. D. Neece, Development of a chlorine mechanism for use in the carbon bond IV chemistry model, *J. Geophys. Res.: Atmos.*, 2003, **108**(D4), DOI: [10.1029/2002jd002432](https://doi.org/10.1029/2002jd002432).

47 W. P. L. Carter, D. R. Cocker, D. R. Fitz, I. L. Malkina, K. Bumiller, C. G. Sauer, J. T. Pisano, C. Bufalino and C. Song, A new environmental chamber for evaluation of gas-phase chemical mechanisms and secondary aerosol formation, *Atmos. Environ.*, 2005, **39**, 7768–7788.

48 M. Huang, W. Zhang, X. Gu, C. Hu, W. Zhao, Z. Wang and L. Fang, Size distribution and chemical composition of secondary organic aerosol formed from Cl-initiated oxidation of toluene, *J. Environ. Sci.*, 2012, **24**, 860–864.

49 C. Bloss, V. Wagner, M. E. Jenkin, R. Volkamer, W. J. Bloss, J. D. Lee, D. E. Heard, K. Wirtz, M. Martin-Reviejo, G. Rea, J. C. Wenger and M. J. Pilling, Development of a detailed chemical mechanism (MCMv3.1) for the atmospheric oxidation of aromatic hydrocarbons, *Atmos. Chem. Phys.*, 2005, **5**, 641–664.



50 R. H. Schwantes, K. A. Schilling, R. C. McVay, H. Lignell, M. M. Coggon, X. Zhang, P. O. Wennberg and J. H. Seinfeld, Formation of highly oxygenated low-volatility products from cresol oxidation, *Atmos. Chem. Phys.*, 2017, **17**, 3453–3474.

51 A. W. Birdsall, J. F. Andreoni and M. J. Elrod, Investigation of the Role of Bicyclic Peroxy Radicals in the Oxidation Mechanism of Toluene, *J. Phys. Chem. A*, 2010, **114**, 10655–10663.

52 M. M. Maricq, J. J. Szente, E. W. Kaiser and J. Shi, Reaction of Chlorine Atoms with Methylperoxy and Ethylperoxy Radicals, *J. Phys. Chem.*, 1994, **98**, 2083.

53 R. S. Karlsson, J. J. Szente, J. C. Ball and M. M. Maricq, Homogeneous aerosol formation by the chlorine atom initiated oxidation of toluene, *J. Phys. Chem. A*, 2001, **105**, 82–96.

54 N. L. Ng, M. R. Canagaratna, Q. Zhang, J. L. Jimenez, J. Tian, I. M. Ulbrich, J. H. Kroll, K. S. Docherty, P. S. Chhabra, R. Bahreini, S. M. Murphy, J. H. Seinfeld, L. Hildebrandt, N. M. Donahue, P. F. Decarlo, V. A. Lanz, A. S. H. Prévôt, E. Dinar, Y. Rudich and D. R. Worsnop, Organic aerosol components observed in Northern Hemispheric datasets from Aerosol Mass Spectrometry, *Atmos. Chem. Phys.*, 2010, **10**, 4625–4641.

55 C. L. Loza, P. S. Chhabra, L. D. Yee, J. S. Craven, R. C. Flagan and J. H. Seinfeld, Chemical aging of m-xylene secondary organic aerosol: laboratory chamber study, *Atmos. Chem. Phys.*, 2012, **12**, 151–167.

56 P. S. Chhabra, N. L. Ng, M. R. Canagaratna, A. L. Corrigan, L. M. Russell, D. R. Worsnop, R. C. Flagan and J. H. Seinfeld, Elemental composition and oxidation of chamber organic aerosol, *Atmos. Chem. Phys.*, 2011, **11**, 8827–8845.

57 M. L. Hinks, J. Montoya-Aguilera, L. Ellison, P. Lin, A. Laskin, J. Laskin, M. Shiraiwa, D. Dabdub and S. A. Nizkorodov, Effect of relative humidity on the composition of secondary organic aerosol from the oxidation of toluene, *Atmos. Chem. Phys.*, 2018, **18**, 1643–1652.

58 T. B. Nguyen, P. J. Roach, J. Laskin, A. Laskin and S. A. Nizkorodov, Effect of humidity on the composition of isoprene photooxidation secondary organic aerosol, *Atmos. Chem. Phys.*, 2011, **11**, 6931–6944.

